https://doi.org/10.1016/j.chempr.2017.01.005

A Catalytic Etching-Wetting-Dewetting Mechanism in Formation of Hollow Graphitic Carbon Fiber

Yuming Chen,[§] Lu Qiu,[‡] Xiaoyan Li,[§] Qianqian Li,[†] Jichen Dong,[‡] Hongtao Wang,[†] Haimin Yao,[§] Feng Ding*[‡] and Limin Zhou*[§]

[§]Department of Mechanical Engineering and [‡]Institute of Textile & Clothing, The Hong Kong Polytechnic University, Hong Kong, China.

[†]Institute of Applied Mechanics, Zhejiang University, Hangzhou 310027, China.

Supporting Information Placeholder

ABSTRACT: Hollow graphitic carbon nanofibers (HGCNFs) have great promise in many important applications such as catalysis, sensors, energy storage, gas separation and electronic devices. Here we report a catalytic etching-wetting-dewetting mechanism in synthesizing the HGCNFs with both hollow spherical-like and tunnel-like pores. With *in situ* transmission electron microscope imaging, we show that the spherical pores are formed by the evaporation of encapsulated Ni on the surface of amorphous carbon nanofiber while the hollow tunnels are developed through continuous etching of the amorphous carbon under catalysis of Ni nanoparticles. Theoretical calculations and simulations reveal that continuous tunnel etching is driven by the wetting-to-dewetting transition of the Ni-tunnel wall interaction during the catalytic graphitization of amorphous carbon wall.

The synthetic strategy of hollow graphitic carbon nanofibers (HGCNFs) with nanometer sized pores or channels is believed important for many applications, for example, as the catalyst or sensor supports,[1-7] hydrogen-storage materials,[8] for gas separation,[9] and in electronic and electrochemical devices[10,11] due to their distinctive features of one-dimensional (1D) structures, high structural and thermal stability, high surface area, and high electric and thermal conductivities. Several methods, such as the chemical vapor deposition (CVD) approach,[12-14] hydrothermal method,[15-18] and electrospinning technique have been developed to synthesize HGCNFs.[19-23] For example, graphitic carbon nanotubes (CNTs) and porous graphitic carbon nanofibers (CNFs) can be synthesized by decomposing gas, such as methane and acetylene, over supported transition metal nanocrystals (e.g., Ni, Co, Fe, or their hybrids);[12,13] the Te-nanowire directed hydrothermal method provides opportunities for developing 1D CNFs;[15] and porous CNTs or CNFs can also be synthesized with electrospinning polymer-based precursor solutions by using single, coaxial, or triple coaxial nozzles, followed by a heating treatment for carbonizing the polymer.[19-22] Recent research has proven that these prepared 1D carbon nanostructures show excellent performance in electronic devices, supercapacitors, and lithium-based batteries.[12,13,15,21] However, the above-mentioned fabrication methods still suffer from several inherent challenges. For example, with the CVD approach and hydrothermal method, it is difficult to control the pore number and diameter (or hollow size) of the resulting carbon materials. Nanostructured carbon prepared by hydrothermal method or electrospinning technique has a low degree of graphitization, giving rise to low conductivity.

In this communication, we present a novel approach to control the Ni diffusion and vaporization in the electrospun amorphous carbon nanofibers during Joule heating to produce HGCNFs with both hollow tunnels and spherical pores (Figure S-1 and Figure 1). Because the content and size of the Ni particles can be easily controlled in such a process and Ni has the high capacity to catalyze the transformation from amorphous carbon to high-quality graphitic carbon, it is possible to synthesize HGCNFs with controlled pore size, pore density and high electric and thermal conductivities.

By using transmission electron microscope (TEM), the formation process of the HGCNFs can be *in situ* observed. As shown in Figure S-1, a single electrospun Ni-amorphous carbon composite nanofiber is attached to a gold rod to form a loop circuit. The *I-V* measurements (voltage and current) is carried out using a Keithley 2420 source meter.

Figure 1a shows a few Ni nanoparticles (with diameter ranging from 15 to 20 nm) encapsulated in graphitic nanospheres in a Ni-carbon composite nanofiber (Figure S-2).[23,24] Only the carbon atoms around the Ni particles are in the graphitic form while those far from Ni particles remain amorphous, confirming the Ni's well-known catalytic role in graphitization as exhibited in CNT or graphene synthesis. When a voltage of 2.7 V (corresponding current is 65 μA) is applied, the Ni nanoparticles on the surface of the fiber quickly disappear, resulting in hollow spheres with a graphitic shell (Figure 1b), whereas those inside the fiber can diffuse a certain distance before being totally evaporated, giving rise to the graphitic-walled tunnels behind (Figures 1b-1f). Such distinct behaviors between the superficial and internal Ni particles suggest that accessibility to the open space of Ni nanoparticle is crucial for its evaporation.

***In situ* TEM.** To further address the process of Ni particles' diffusion in the amorphous carbon fiber, we analyze the behavior of a large Ni particle with diameters of ~150 nm (as their rate of evaporation is relatively slow and thus both the transformation and evaporation processes can be clearly observed). These images demonstrate an etching-elongation-broken-contraction (EEBC) process accompanied by the evaporation of the Ni particle (Figure 2). Firstly, when a voltage of 3.5 V is applied, the Ni particle

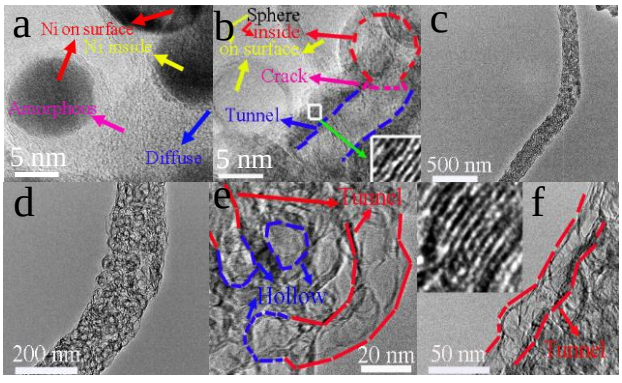

Figure 1. TEM and HRTEM images of (a) Ni-carbon composite and (b) HGCNF obtained by applying a voltage of 2.7 V between Ni-carbon composite nanofiber and Au rod. (c-f) Low- and high-magnification TEM and HRTEM images of HGCNFs with hollow sphere and tunnel structure.

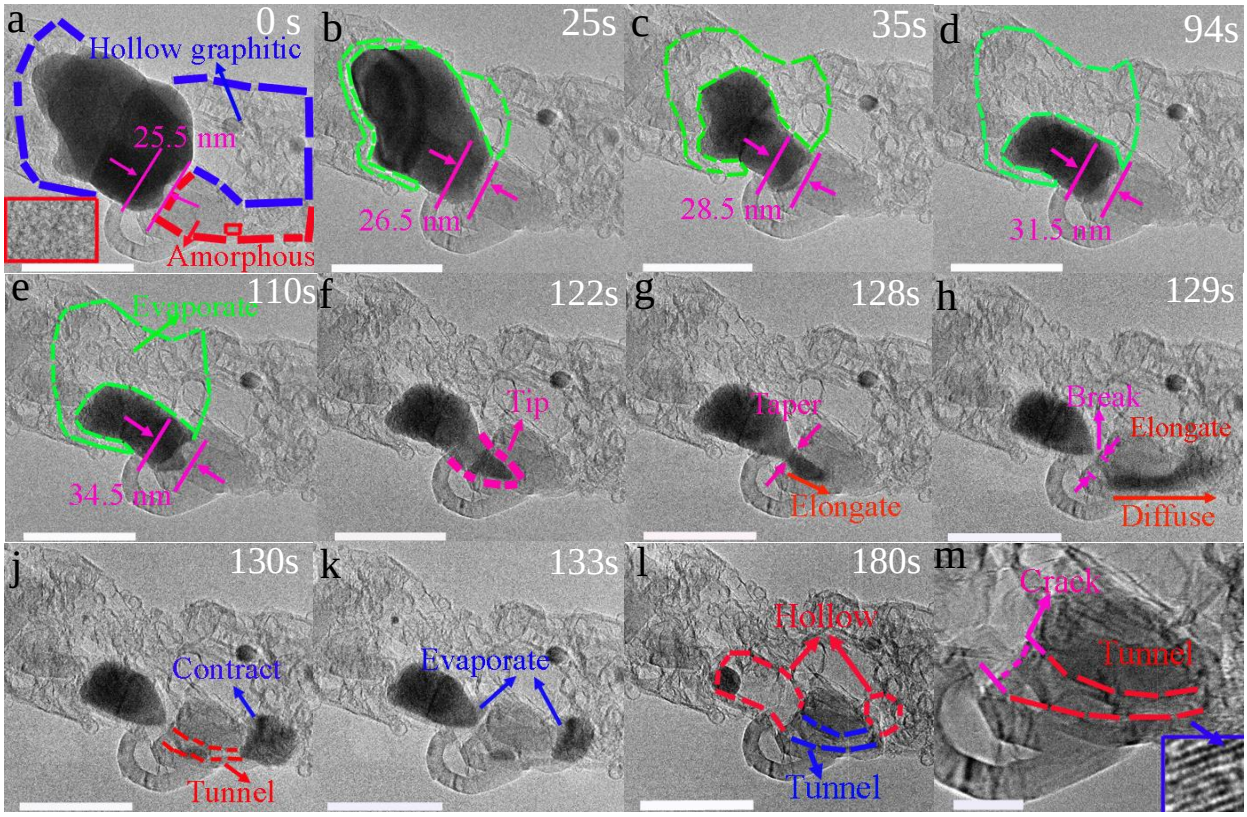

Figure 2. TEM images showing the etching-elongation-broken-contraction (EEBC) process accompanied by the evaporation of the Ni particle. The images are acquired *in situ* with a voltage of 3.5 V and current of 99 μA. Scale bar, (a-l) 100 nm and (m) 10 nm. Images a to m show the sequence of the formation of hollow graphitic sphere and tunnel structure.

begins to evaporate and becomes smaller and smaller as is indicated by the green dotted line. Meanwhile, a part of the Ni particle that is attached to the amorphous carbon continuously passes through the amorphous carbon and forms a 9 nm-long Ni tip embedded into the amorphous carbon (Figures 2a-2e). Then, the size of the crack increases (Figure 2f), followed by the tapering of a part of the Ni near the crack (Figure 2g). Then, the tip of the Ni breaks apart from the maternal Ni particle and the child Ni elongates and keeps moving forward (Figure 2h). Due to the continuous etching of the amorphous carbon on the path of the Ni's movement, an empty tunnel with graphitic walls is formed (Figures 2j and 2m).[25] The graphitic wall of the tunnel is formed by the catalytic transformation from amorphous carbon to graphitic carbon. The driving force of the whole process shown in Figure 2 can be ascribed to the high temperature caused by the Joule heating (evidenced by the evaporation of the Ni) and catalytic conversion of amorphous carbon into more stable graphitic carbon.[26] Finally, both separated Ni particles completely evaporated, leaving a graphitic-walled tunnel inside the carbon fiber (Figures 2k and 2l). The low- and high-magnification TEM and HRTEM images in Figures 1c-1f show that the HGCNFs with hollow spheres and tunnels can be obtained with the developed Joule heating mechanism. Additionally, the relationship between the applied voltage/current and the evaporated size of the Ni particles is shown in Figure S-3. With the increase of the Ni particle size, the voltage and current also need to be increased in order to evaporate the larger Ni particle. When a higher voltage of 5.8 V is applied, all the Ni particles evaporate in the order of size, from small to large (Figure S-4). In addition, a linear relationship is observed between *I* and *V* is shown (Figure S-5).

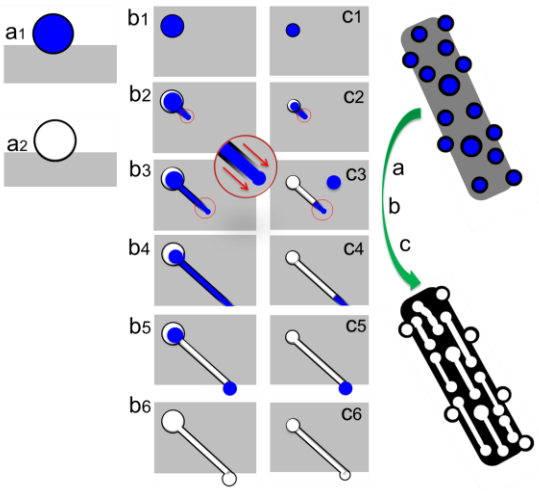

Figure 3. Illustration of three processes that form the pores and tunnels in the amorphous carbon fiber:(a1→a2) evaporation of the Ni from the surface of the fiber leads to a spherical graphitic pore; (b1→b6) the etching-elongation-breaking-contraction (EEBC) process accompanied with the evaporation of the Ni forms a graphitic tunnel in the fiber; (c1→c6) the etching-elongation-contraction process of forming a tunnel in the fiber. The gray, black and blue represent the amorphous carbon, graphitic carbon and Ni, respectively in all panels. The insert shows the level of graphitization of the tunnel wall, where a transition from amorphous carbon (gray) to highly graphitized carbon (black) can be clearly seen. The driving force from the low adhesion wall to the high adhesion tip is also shown by arrows.

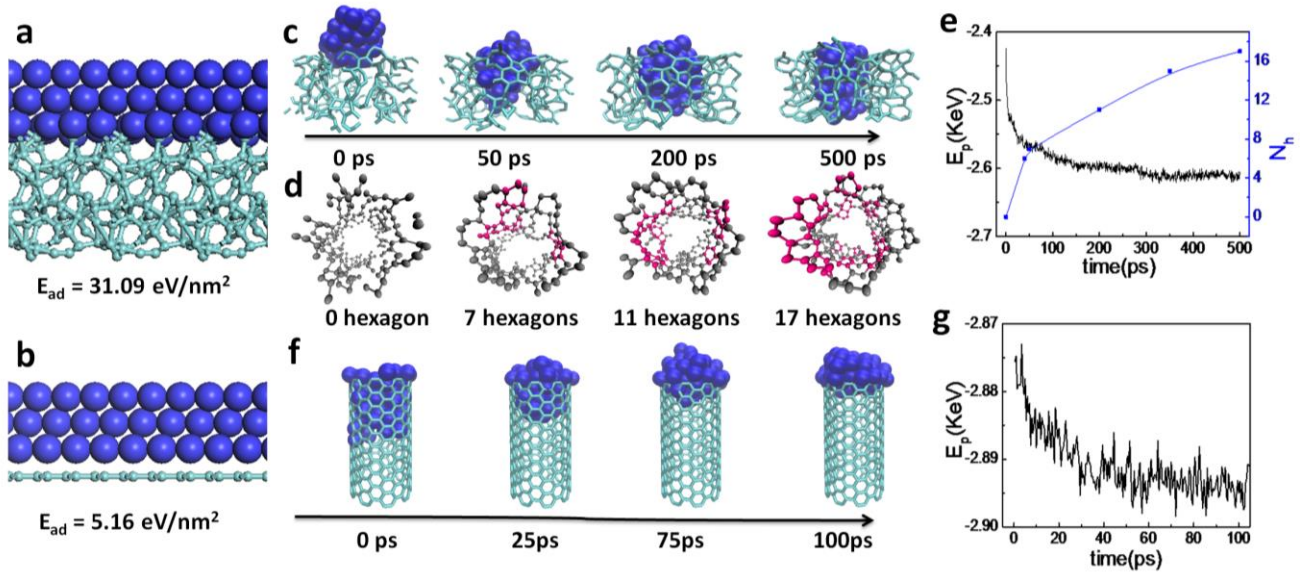

Figure 4. The mechanism of wetting and dewetting of Ni in amorphous carbon and high quality graphitic carbon. a and b, adhesion between Ni(111) surface and amorphous carbon or graphene calculated by density functional theory method. **c**, snapshots taken during the MD simulation of the wetting of the Ni into a hole in amorphous carbon and, **d**, the evolution of the wall of the hole in the amorphous carbon during the annealing process. **e**, The energy and the number of hexagons on the wall of hole of amorphous carbon during the simulation. **f**, Snapshots taken during the MD simulation of a dewetting procedure of Ni catalyst from a high quality CNT, representing a hole with high quality graphitic carbon wall. **g**, The energy *vs*. time curve during the dewetting procedure.

The EEBC procedure together with the formation of the spherical pores on the fiber surface and the etching-elongation-contraction (EEC) process, where all Ni particles move to another side of the tunnel, is illustrated in Figure 3. For both EEBC and EEC procedures, the Ni particle firstly elongates and spills into the etched tunnel and, latterly, the elongated Ni inside the tunnel becomes unstable and retreats from the tunnel. It is apparent that the Ni-tunnel wall interaction must undergo a transition from wetting to dewetting, where the wetting interaction is responsible for the filling of Ni into the tunnel and the dewetting leads to the retreat of the Ni from the tunnel. The transition between transition metal and graphitic carbon has been broadly observed in the growth of CNT or CNF,[27,28] but such process and corresponding mechanism has never been reported in amorphous carbon. The transition in graphitic carbon has been attributed to the weakened metal-graphitic wall adhesion caused by the solubility of C in the transition metal.[28,29] But such mechanism cannot be applied to the transition observed in our study, where the wetting process is accompanied by the simultaneous etching of amorphous carbon and therefore the carbon solubility inside the Ni must be very high. And the dewetting occurs after a long term annealing of Ni inside the tunnel, which must result in the precipitation of the dissolved carbon from Ni and therefore low carbon solubility in Ni. Such a procedure is in contrast to the observation in CNT or CNF growth, where the wetting and dewetting occur when the metal has either low or high carbon solubility respectively. So, the underlying mechanism and driving force leading to the EEBC and EEC behavior of the Ni in amorphous carbon must be different.

To shed light on the driving force of the EEBC and EEC of the Ni particle in amorphous carbon, here we propose another mechanism of the wetting-to-dewetting transition.

We notice that the adhesion between amorphous carbon and transition metal is much higher than that between metal and graphitic carbon because of the active dangling bonds hanging on the surface of the amorphous carbon. As shown in Figures 4a and 4b, the calculated adhesion between the amorphous carbon and the Ni(111) surface is 31.09 eV/nm^2, which is about five times greater than that between Ni(111) surface and perfect graphene, which is only 5.16 eV/nm^2.

As seen in a molecular dynamic (MD) simulation (Figure 4c, see SI for more details), the strong adhesion between the Ni and amorphous carbon is sufficient to drive a Ni particle into a hole in the amorphous carbon as the energy of the whole system keeps dropping during the whole wetting process (Figure 4e). Additionally, we observe a structural evolution of the hole wall in amorphous carbon during the simulation. As a consequence of the graphitization, the number of hexagons in the wall of the hole increases from zero to 17 within 500 ps at the temperature of 2000 K (Figures 4d and 4e). The graphitization of the amorphous carbon wall can be ascribed to the catalytic healing of defects on the interface between Ni and amorphous carbon.[30]

Different from the wetting of Ni in a hole of amorphous carbon, a Ni particle inside a high quality CNT wall is energetically less stable and prefers to retreat to the outside and gathers at the open end of the CNT (Figures 4f and 4g). Such a dewetting procedure is attributed to the low adhesion between the Ni and high quality graphitic wall.

From above calculations and MD simulations, we can propose a new mechanism of the EEBC and EEC by considering the wetting-to-dewetting transition between Ni and the wall of hole in amorphous carbon as the driving force (Figure 3):

a) The etching of amorphous carbon by Ni leads hole or dent with amorphous carbon wall, in which the adhesion to the Ni catalyst is very high (Figures 3b2 and c2);

b) Therefore, the wetting of the Ni into the hole of amorphous carbon occurred and drives the elongation of the Ni particle and the continuous etching of the amorphous carbon to form a long tunnel (Figures 3b3 and c3);

c) Simultaneously, the wall of the tunnel in the amorphous carbon undergoes a transition from amorphous structure to graphitic structure due to the catalytic effect of transition metal at high temperature. With the graphitization of the wall, the adhesion between Ni and the hole becomes progressively weaker.

d) The wall formed has higher quality and weaker interaction with the Ni and therefore the adhesion gradient (or the gradient of wettability) drives the motion of the Ni far into the deep of the amorphous carbon until all Ni atoms evaporate away or reaches the surface of the fiber and trapped there;

e) Once the quality of the wall of the whole tunnel becomes high enough, the adhesion drops below a critical value and the Ni inside the tunnel becomes unstable. Then the retraction of Ni from the tunnel will suddenly occurs as a consequence of dewetting (Figures 3b5 and c5). If there are still Ni on the entrance of the tunnel, the whole Ni catalyst will break into two as the EEBC process shown in Figure 3b5. Otherwise, if all the Ni goes into the tunnel, the process of EEC will be seen (Figures 3c1-c6).

In summary, we develop an interesting and versatile method based on the Joule heating mechanism for synthesizing hollow graphitic carbon nanofibers. Our in situ observations and theoretical explorations reveal that the formation of the hollow tunnels inside the fibers is caused by an etching-elongation-contraction or etching-elongation-broken-contraction process during the evaporation of Ni from Ni-carbon composite nanofibers. The wetting to dewetting transition between catalyst and tunnel wall serves as the driving force of both processes and a new mechanism of the transition is developed based on both DFT calculation and MD simulations. The energy from Joule heating can reach a very high level. Our ongoing work is focused on other transition metals (e.g., Fe and Co) that can also serve as catalysts for the formation and mass production of the HGCNFs. The simple synthetic process can be extended to the production of other porous graphitic carbon nanomaterials for applications in catalyst and sensor supports, hydrogen-storage materials, gas separation, and electronic and electrochemical devices.

ASSOCIATED CONTENT

Supporting Information

Detailed experimental and simulation methods and other materials. This material is available free of charge via the Internet at http://pubs.acs.org.

AUTHOR INFORMATION

*Corresponding Authors

tcfding@polyu.edu.hk and mmlmzhou@polyu.edu.hk

Notes

The authors declare no competing financial interests.

ACKNOWLEDGMENT

The authors are grateful for the support from the Research Grants Council of the Hong Kong Special Administration Region (Grant: PolyU 5312/12E) and the Hong Kong Polytechnic University (Grants:G-YK47;G-YX4Y). HW acknowledges the financial supports from National Science Foundation of China (Grant No.11322219), National Program for Special Support of Top-Notch Young Professionals and Fundamental Research Funds for the Central University (2014XZZX003-19).

REFERENCES

(1) Iliafar, S.; Mittal, J.; Vezenov, D.; Jagota A. *J. Am. Chem. Soc.* **2014**, *136*, 12947-12957.

(2) Chen, Y. M.; Li, X. Y.; Park, K. S.; Song, J.; Hong, J. H.; Zhou, L. M.; Mai, Y.-W.; Huang, H. T.; Goodenough, J. B. *J. Am. Chem. Soc.* **2013**, *135*, 16280-16283.

(3) Rance, G. A.; Solomonsz, W. A.; Khlobystov, A. N. *Chem.Commun*. 2013, 49, 1067-1069.

(4) Lebedeva, M. A.; Chamberlain, T. W.; Schröder, M.; Khlobystov, A. N. *Chem. Mater*. 2014, 26, 6461-6466.

(5) Gorgoll, R. M.; Yücelen, M.; Kumamoto, A.; Shibata, N.; Harano, K.; Nakamura, E. *J. Am. Chem. Soc.* **2015**, *137*, 3474-3477.

(6) Nakamura, E., Koshino, M.; Saito, T.; Niimi, Y.; Suenaga, K.; Matsuo, Y. *J. Am. Chem. Soc.* **2011**, *133*, 14151-14153.

(7) Lebedeva, I. V.; Chamberlain, T. W.; Popov, A. M.; Knizhnik, A. A.; Zoberbier. T.; Biskupek, J.; Kaiser, U.; Khlobystov. A. N. *Nanoscale* **2014**, 6, 14877-14890.

(8) Yang, S. J.; Choi, J. Y.; Chae, H. K.; Cho, J. H.; Nahm, K. S.; Park, C. R. *Chem. Mater.* **2009**, *21*, 1893-1897.

(9) Yang, X. H.; Yuan, L. X.; Peterson, V. K.; Minett, A. I.; Zhao, M.; Kirby, N.; Mudie, S.; Harris, A. *ACS Appl. Mater. Interfaces* **2013**, *5*, 3063-3070.

(10) Ma, T. Y.; Dai, S.; Jaroniec, M.; Qiao, S. Z. *J. Am. Chem. Soc.* **2014**, *136*, 13925-13931.

(11) Cui, C. J.; Qian, W. Z.; Yu, Y. T.; Kong, C. Y.; Yu, B.; Xiang, L.; Wei, F. *J. Am. Chem. Soc.* **2014**, *136*, 2256-2259.

(12) Fan, Z. J.; Yan, J.; Wei, T.; Ning, G. Q.; Zhi, L. J.; Liu, J. C.; Cao, D. X.; Wang, G. L.; Wei, F. *ACS Nano* **2011**, *5*, 2787-2794.

(13) Wu, Z. S.; Ren, W. C.; Xu, L.; Li, F.; Cheng, H. M. *ACS Nano* **2011**, 5, 5463-5471.

(14) Wen, Z.; Ci, S.; Hou, Y.; Chen, J. *Angew. Chem., Int. Ed.* **2014**, 53, 6496-6500.

(15) Zhang, G. Q.; Wu, H. B.; Hoster, H. E.; Lou, X. W. *Energy Environ. Sci.* **2014**, *7*, 302-305.

(16) Liang, H. W.; Guan, Q. F.; Chen, L. F.; Zhu, Z.; Zhang, W. J.; Yu, S. H. *Angew. Chem., Int. Ed.* 2012, **51**, 5101-5105.

(17) Zhang, G. Q.; Xia, B. Y.; Xiao, C.; Yu, L.; Wang, X.; Xie, Y.; Lou, X. W. *Angew. Chem., Int. Ed.* **2013**, *52*, 8643-8647.

(18) Zhang, G. Q.; Yu, L.; Hoster, H. E.; Lou, X. W. *Nanoscale* **2013**, *5*, 877-881.

(19) Chen, Y. M.; Lu, Z. G.; Zhou, L. M.; Mai, Y. W.; Huang, H. T. *Nanoscale* **2012**, *4*, 6800-6805.

(20) Chen, Y. M.; Lu, Z. G.; Zhou, L. M.; Mai, Y. W.; Huang, H. T. *Energy Environ. Sci.* **2012**, *5*, 7898-7902.

(21) Chen, Y. M.; Li, X. Y.; Zhou, X. Y.; Yao, H. M.; Huang, H. T.; Mai, Y. W.; Zhou, L. M. *Energy Environ. Sci.* **2014**, *7*, 2689-2696.

(22) Zhang, B.; Yu, Y.; Xu, Z. L.; Abouali, S.; Akbari, M.; He, Y. B.; Kang, F. Y.; Kim, J. K. *Adv. Energy Mater*. **2014**, *4*, 1301448-1301457.

(23) Thess, A.; Lee, R.; Nikolaev, P.; Dai, H. J.; Petit, P.; Robert, J.; Xu, C. H.; Lee, Y. H.; Kim, S. G.; Rinzler, A. G.; Colbert, D. T.; Scuseria, G. E.; Tománek, D.; Fischer, J. E.; Smalley, R. E. *Science* **1996**, *273*, 483-487.

(24) Shang, S. M.; Yang, X. M.; Tao, X. M. *Polymer* **2009**, *50*, 2815-2818.

(25) Helveg, S.; Lopez-Cortes, C.; Sehested, J.; Hansen, P. L.; Clausen, B. S.; Rostrup-Nielsen, J. R.; Abild-Pedersen, F.; Nørskov, J. K. *Nature* **2004**, *427*, 426-429.

(26) Anton, R. *Carbon* **2008**, *46*, 656-662.

(27) Hofmann, S.; Sharma, R.; Ducati, C.; Du, G. H.; Mattevi, C.; Cepek, C.; Cantoro, M.; Pisana, S.; Parvez, A.; Cervantes-Sodi, F.; Ferrari, A. C.; Dunin-Borkowski, R.; Lizzit, S.; Petaccia, L.; Goldoni, A.; Robertson, J. *Nano Lett.* **2007**, *7*, 602-608.

(28) Pigos, E.; Penev, E. S.; Ribas, M. A.; Sharma, R.; Yakobson, B. I.; Harutyunyan, A. R. *ACS Nano* **2011**, *5*, 10096-10101.

(29) Diarra, M.; Zappelli, A.; Amara, H.; Ducastelle, F.; Bichara, C. *Phys. Rev. Lett*. **2012**, *109*, 185501.

(30) Yuan, Q. H.; Xu, Z. P.; Yakobson, B. I.; Ding, F. *Phys. Rev. Lett*. **2012**, *108*, 245505.

TOC Graphic

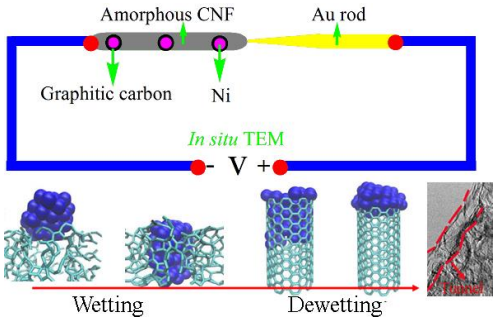
Amorphous CNF
Au rod
Graphitic carbon
Ni
In situ TEM
- V +
Wetting
Dewetting